

Phase-resolved imaging of spin-wave eigenmodes in nanoscale ellipses

Cheng Cheng,¹ William E. Bailey^{1*}

¹Materials Science and Engineering,
Department of Applied Physics and Applied Mathematics, Columbia University,
500 West 120th St., New York, NY 10027, USA

*To whom correspondence should be addressed; E-mail: web54@columbia.edu

Spin waves are thought to possess different GHz eigenmodes when confined to magnetic nanostructures[1]. Until now, it has not been possible to image these eigenmodes without sacrificing information on the spin-wave phase[2, 3], crucial for the response of spin electronic devices[4]. Here we demonstrate phase-resolved measurements of spin-wave eigenmodes in single and coupled $1000\text{ nm} \times 500\text{ nm} \times 20\text{ nm}$ $\text{Ni}_{81}\text{Fe}_{19}$ ellipses, a simple building-block of nanoscale magnetic devices, using the high spatiotemporal resolution of time-resolved scanning transmission x-ray microscopy[5]. Predicted degenerate modes[1] have been separated experimentally for the first time.

The dynamics of magnetization in ferromagnetic nanostructures are of great interest for GHz spin-electronic devices. In these devices, whether magnetization moves in response to pulsed excitation (as in spin-torque magnetic random access memory, STT-MRAM)[6, 7] or auto-oscillation (as in a spin-torque or spin-Hall oscillator)[8, 9], available spin-wave eigenmodes give the low-power basis for the response. Here the complex, or phase-sensitive nature of spin-wave eigenmodes is essential: departures from uniform spin-wave phase across the element will tend to decrease the amplitude of the magnetoresistive response, potentially to zero.

Micromagnetic calculations[1, 10] predict specific fundamental spin-wave modes at GHz frequencies in nanostructures. In a soft magnetic structure with confined geometries and negligible magnetocrystalline anisotropy, the spin-wave modes spectrum is determined by the effective magnetic field, which is the sum of external bias field, dipolar interaction, exchange interaction between adjacent spins, and demagnetizing field intro-

duced by the shape. The modes of nanoscale, thin-film ellipses have been of particular interest, both for scientific studies and spin-electronic devices, because of their simplicity. Ellipsoids, which have dimensions varying along all three cartesian axes, are known to have uniform demagnetizing fields (constant self-energy) in the uniformly magnetized state, promoting single-domain (Stoner-Wolfarth) switching[11, 12]. For the ellipsoid, the lowest-energy mode is the uniform mode, with all magnetization precessing with equal phase and amplitude[13].

Thin-film ellipses, which have uniform thickness and elliptical in-plane shape, are the closest realization of ellipsoids in lithography. For short-axis sample dimensions less than a few multiples of the domain-wall width (~ 200 nm), the remanent state is nearly uniformly magnetized[1]. This magnetization configuration is convenient for GHz devices, since both the effective field from shape anisotropy (determining magnetic stiffness) and the resonant frequency of the most uniform eigenmode can be tuned through the aspect ratio. Nanoscale, elliptical ferromagnet/ insulator/ ferromagnet heterostructures are thus widely used in spin-torque devices[6, 7, 8, 9]. However, unlike ideal ellipsoids, the demagnetizing field is raised at the ends of the thin-film ellipse, resulting in an 'edge' mode occurring at the lowest frequency of the spin-wave spectrum, and the 'uniform' mode is shifted to a higher frequency. It has also been predicted by micromagnetic calculations that degenerate 'edge' modes occur under excitation fields with different symmetries, having the same distribution of magnetization precession amplitude while the phase reflects the symmetry of the driving field[1]. These degenerate modes have not been resolved experimentally.

It has not yet been possible to image complex spin-wave eigenmodes in nanoscale, nearly uniformly magnetized structures such as ellipses. This has been a challenging problem due to the fine spatial resolution and small-angle moment sensitivity required. Visible-light microscopies[9, 14, 15, 16, 17, 18] have provided powerful techniques to in-

investigate complex eigenmodes in larger structures, set by the diffraction limit of 200-250 nm. Complex spin-wave eigenmodes have been imaged using visible light Kerr microscopy in 4 micron ring structures supporting high-angle domains or vortex states[15]. Studies of spin-wave eigenmodes in nearly uniformly magnetized submicrometer ellipses/circular disks have been enabled through the recent development of near-field optical techniques with small aperture[2] and ferromagnetic resonance force microscopy[3]. Nevertheless, these latter two techniques can access only the scalar eigenmodes, losing the phase information critical for device operation[4]. On the other hand, time-resolved x-ray microscopies have high spatial resolution, potentially to 15 nm[19], due to the short wavelength of soft x-rays, providing intriguing observations of magnetization dynamics in micrometer-size ferromagnetic structures. Time-resolved x-ray microscopy studies of magnetization dynamics have, until now, focused on large-angle dynamics with high magnetic contrast, such as vortex gyration[20, 21].

In this context we present the two-dimensional (2D) mapping of spin-wave modes in isolated and coupled nearly-single-domain submicrometer magnetic ellipses using time-resolved scanning transmission x-ray microscopy (TR-STXM), revealing clear phase information on the symmetry of the spin-wave modes. The origin of magnetic contrast in STXM is x-ray magnetic circular dichroism (XMCD)[22], which yields magnetic moment (\mathbf{M})-dependent absorption of circularly polarized x-ray at transition metal $L_{2,3}$ edges. Soft x-rays have the advantage of element-specific XMCD, making layer-resolved imaging possible in thin film stacks provided each magnetic layer has different composition. Improved spatial resolution up to ~ 15 nm is available with advanced optics[19]. Temporal resolution of 2 ps has been achieved using the radio frequency (rf)-pump/synchrotron-probe technique in TR-XMCD[4, 23]. We carried out TR-STXM measurements at the Canadian Light Source (CLS), soft x-ray spectromicroscopy beamline 10ID-1 (SM, x-ray spot

size 40 nm). The experimental setup is described in detail elsewhere[5] and summarized in *Methods*.

We show results from four separate nanostructures made from two distinct multilayer stacks. The samples are fabricated on top of a 200 nm thick Si_3N_4 membrane to allow x-ray transmission. We define the ellipses by e-beam lithography and liftoff, patterning dimensions of two types of ellipses that we focus our attention on, $1000 \text{ nm} \times 500 \text{ nm}$ (*A*) and $1000 \text{ nm} \times 600 \text{ nm}$ (*B*). Increasing the short-axis dimension in *B* shifts the modes to lower frequency, as expected through reduction of the shape anisotropy field and according to our micromagnetic simulations (using NMag[24], see *Methods*). The symmetry of the excited spin-wave mode within the ellipse, and thus the spin-wave phase profile, depends on the symmetry of the driving rf field. More specifically, if the driving field is antisymmetric about the midline of the ellipse along the long axis, the phase is antisymmetric; under uniform excitation, the phase is symmetric about the midline.

To distinguish between these degenerate spin-wave modes, we generate antisymmetric and uniform rf excitations through the introduction and omission of conductive overlayers, respectively, in heterostructures deposited by ultrahigh vacuum (UHV) magnetron sputtering. The first stack configuration (*I*) is Ta (3 nm)/ $\text{Ni}_{81}\text{Fe}_{19}$ (20 nm)/ Ta (3 nm) \rightarrow patterning \rightarrow /Cu (15 nm), shown in Fig.1(a). The seed Ta (3 nm) improves film adhesion to the substrate and enhances homogeneity of the ferromagnetic layer, $\text{Ni}_{81}\text{Fe}_{19}$ (20 nm). The top Ta (3 nm) prevents oxidation of the magnetic structure. After the liftoff process, we deposited an extra layer of 15 nm Cu on the sample wafer to induce antisymmetric rf excitation, as explained in Fig.1(b) and *supplementary information*. Because of the rf electrical field perpendicular to the sample plane from the coplanar waveguide (CPW)[25], an extra transverse rf magnetic field ($\sim 5 \text{ Oe}$) is introduced by the eddy cur-

rent in the Cu layer, which compensates the direct transverse rf magnetic field (~ 1 Oe) from the CPW and causes odd excitation. The second stack configuration (*II*) is Ta (2 nm)/ Ni₈₁Fe₁₉ (20 nm)/ SiO₂ (2 nm), where Ta (2 nm) is the seed and SiO₂ (2 nm) is the cap, shown in Fig.1(c). The excitation field is uniform, generated by the CPW, as explained in Fig.1(d). The ferromagnetic layers in both configurations are identical, sputtered under optimized conditions (Ar 1.2 mTorr, DC 400 V, base pressure 2×10^{-9} Torr) for soft magnetic properties. The differences in the seed and cap layers do not have significant influence on magnetic properties. Immediately before taking the TR-STXM measurements, we magnetized the samples along the long axis of the ellipse using a 0.3 T permanent magnet. Due to the large shape anisotropy (~ 200 Oe) in these nanoscale structures, the ellipses remain nearly saturated after the magnet is removed.

Fig.2(a) demonstrates the 'edge' mode we observed in the $1000 \text{ nm} \times 500 \text{ nm} \times 20 \text{ nm}$ Ni₈₁Fe₁₉ sample covered by Cu (15 nm) (*A,I*). The simulations show that the 'edge' mode is the spin-wave eigenmode occurring at the lowest frequency, 2 GHz in this case. It has the highest amplitude of magnetization precession at the two tips of the ellipse, and shows the same amplitude distribution under antisymmetric (odd) and uniform (even) rf excitations. The left image in Fig.2(a) is the simulated map of magnetization precession amplitude at 2 GHz under zero bias, illustrating the 'edge' mode. The right panel of Fig.2(a) demonstrates the experimental data under 2 GHz odd rf excitation. The image labeled 0 Oe is taken under zero bias, showing a reasonable match with the simulated image, the highest precession amplitude concentrated at the tips of the ellipse. There is also strong evidence in the corresponding phase map that the observed spin-wave mode is antisymmetric about the midline of the element. By applying varying external bias fields using an electromagnet installed in the STXM chamber, we observe changed patterns of magnetization dynamics in the ellipse, as shown in the images labeled -10 Oe, 20 Oe and

40 Oe. In Fig.2(b), we show the experimental data at 2 GHz even excitation for the $1000 \text{ nm} \times 500 \text{ nm} \times 20 \text{ nm}$ $\text{Ni}_{81}\text{Fe}_{19}$ ellipse (A, II) under zero bias, obtained from the second type of layer structure (II) where the Cu (15 nm) overlayer is absent. The amplitude still shows its maximum at the tips, consistent with the simulated image; however, the phase map is clearly symmetric about the midline, in contrast with the 0 Oe experimental image in (a) where we implemented odd excitation. Comparing the amplitudes of the 0 Oe images in Fig.2(a) and (b), we notice the response in the odd excitation case is stronger. This is consistent with our estimation of the eddy-current induced magnetic field, which is about 4 times larger than the transverse magnetic field directly from the CPW. Next, in Fig.2(c), we present a distinctive pattern of spin-wave mode under the same conditions, 2 GHz odd excitation and zero bias, in the wider, $1000 \text{ nm} \times 600 \text{ nm} \times 20 \text{ nm}$ $\text{Ni}_{81}\text{Fe}_{19}$ ellipse (B, I). The left image is the simulated amplitude map and the right panel shows the experimental data of amplitude and phase. Compared with the $1000 \text{ nm} \times 500 \text{ nm} \times 20 \text{ nm}$ $\text{Ni}_{81}\text{Fe}_{19}$ ellipse (A, I), this geometry gives more uniform distribution of the spin precession amplitude. We attribute this to the predicted downshift in frequency of 'edge' and 'uniform' modes, bringing the lower-frequency 'edge' mode further away and the higher-frequency 'uniform' mode closer to resonance at 2 GHz. Reduced shape anisotropy, due to the larger width of the ellipse, leads to lower effective field within the element. Consequently all the spin-wave eigenmodes are shifted towards lower frequencies.

Finally, in Fig.3, we demonstrate the capability of TR-STXM to image the collective spin-wave modes of coupled elliptical structures, for a $1000 \text{ nm} \times 500 \text{ nm} \times 20 \text{ nm}$ $\text{Ni}_{81}\text{Fe}_{19}$ pair under 2 GHz odd excitation ($A \text{ pair}, I$). Consistent with the simulation at zero bias in Fig.3(a), the experimental map of amplitude taken at zero bias (0 Oe), shown in Fig.3(b), shows reduced precessional amplitude in the vertical region where the ellipses overlap and the element pair experiences relatively strong dipolar coupling. In the simulated phase

map, the pair precess in phase where they overlap and show antisymmetric phase at the two further ends; we see such a response in the experimental phase map. We found only qualitative connections between the simulations and the experimental data, most likely due to the complex distribution of the electrical and magnetic fields around and in the pair, introduced by both the short distance between the two ellipses and the 15 nm Cu cover layer. The phase distribution should reflect the symmetry of the excitation rf field in this case. By contrast, the 40 Oe image shows near zero amplitude, indicating that the pair is off-resonance under this bias condition.

From the images demonstrated, we conclude that we are able to detect the small-angle ($< 6^\circ$) dynamics in a nearly saturated nanoscale magnetic structure with 40 nm resolution and clear phase information, and to resolve the different spin-wave eigenmodes and distinguish between degenerate modes with different symmetries which are predicted by micromagnetic simulations. Further extending this technique to multilayered structures with the element-specific and buried-layer imaging capability of soft x-rays, we see enormous potential for the technique to shed light on the dynamics of functional spin-electronic devices, operated near the uniformly magnetized state.

Methods

Experimental setup Fig.4(a) shows the diagram of the experimental setup. The bunched x-ray (energy set to 707.9 eV for maximum XMCD at Fe L_3 edge) repeats at the frequency of 500 MHz with pulse duration of 35 ps. We take the bunch-clock signal as the rf source, send it through the comb generator to obtain the harmonics of 0.5 GHz, then select the desired frequency (2.0 GHz) using a bandpass filter. Thus we have the rf-pump that is synchronized with the x-ray probe. By sending the 2.0 GHz signal

through the delay line (programmable with 1 ps resolution), we define the relative position of the probe and the pump. The power of the rf excitation is tuned by the combination of amplifiers and attenuators, which we fix at +29 dBm before sending to the CPW. The CPW is custom designed with a hole (100 μm diameter) in the center conductor to allow transmission of the x-ray probe. We mount the sample such that the long axis of the $\text{Ni}_{81}\text{Fe}_{19}$ ellipse is aligned with the center conductor (the x -axis), and the magnetization is nearly saturated along the long axis. A custom made electromagnet is installed in the STXM vacuum chamber to apply moderate (tens of Oe) DC bias magnetic field on the sample along the x -axis. When the rf excitation is exerted, the magnetization precesses about the x -axis at a small cone angle. In order to detect this precession by XMCD, we rotate the CPW/sample plane 30° away from the xy -plane to visualize the y' component of the magnetization as the projection of $m_{y'}$ on the z -axis, the propagation direction of the circularly polarized x-ray. For each delay point, we take two images with circular-left (CL) and circular-right (CR) x-rays respectively, and take the difference between the two to enhance the magnetic contrast.

Experimental data Fig.4(b) illustrates the extraction of local magnetization precession amplitude and phase from the TR-STXM images. For each image we fix the scanning step at 14.7 nm and average the local magnetic contrast in a $3\text{-pixel} \times 3\text{-pixel}$ square. The local averaged magnetic contrast at each pixel is plotted as a function of the delay time, as shown in the lower panel of Fig.4(b). We then fit a sinusoidal function to $M(t)$ to extract the amplitude, phase and offset of the oscillation in contrast. The amplitude is converted to cone angle by comparing with the contrast from a sample fully saturated in the y' -axis.

Simulations We define the sample geometry and generate the finite-element mesh using the open source software *Netgen*. The largest mesh size is 5 nm, within the limit of the exchange length of $\text{Ni}_{81}\text{Fe}_{19}$. With the geometry and mesh imported into *NMag*, we start with the sample saturated along the x -direction by setting the magnetization uniformly as $\mathbf{m} = (1, 0, 0)$. To get the remanent state of the sample, we let it relax under zero external field. Because of the large shape anisotropy introduced by the geometry of the elliptical cylinder, the $\text{Ni}_{81}\text{Fe}_{19}$ sample is almost uniformly magnetized along the x -axis at remanence, with only slight dispersion of the magnetization at the two tips of the ellipse.

To obtain the spin-wave modes under zero bias field in the simulation, we use the remanent state of the thin film sample as the static magnetization configuration. A square field pulse (duration ~ 85 ps) of ~ 12 Oe (very small compared with the shape anisotropy as could be inferred from the simulated hysteresis loop) is applied along the y' -axis uniformly over the whole space for even excitation. For odd excitation, the y' -axis field is $+12$ Oe for $x > 0$ and -12 Oe for $x \leq 0$. The magnetization then relaxes after the field pulse, with the Gilbert damping parameter α set to 0.01, until reaching equilibrium. We take the data $\{\mathbf{m}(\mathbf{r}, t)\}$ in the whole sample during the time interval of 2.3 - 4.3 ns with step of 10 ps, and perform a fast Fourier transform (FFT) in each spatial element $d^3\mathbf{r}$ for $m_x(t)$, $m_{y'}(t)$ and $m_{z'}(t)$. The time-domain data of the oscillating magnetization components m_x , $m_{y'}$, $m_{z'}$ are then transformed into the frequency domain, and give the amplitude and phase at each discrete frequency.

References

- [1] R. D. McMichael and M. D. Stiles, Magnetic normal modes of nanoelements, *J. Appl. Phys.* **97**, 10J901 (2005)

- [2] J. Jersch, V. E. Demidov, H. Fuchs, K. Rott, P. Krzysteczko, J. Munchenberger, G. Reiss, and S. O. Demokritov, Mapping of localized spin-wave excitations by near-field Brillouin light scattering, *Appl. Phys. Lett.* **97**, 152502 (2010)
- [3] F. Guo, L. M. Belova, and R. D. McMichael, Spectroscopy and imaging of edge modes in permalloy nanodisks, *Phys. Rev. Lett.* **110**, 107601 (2013)
- [4] W. E. Bailey, C. Cheng, R. Knut, O. Karis, S. Auffret, S. Zohar, D. Keavney, P. Warnicke, J.-S. Lee and D. A. Arena, Detection of microwave phase variation in nanometre-scale magnetic heterostructures, *Nature Comms.* **4**, 2025 (2013)
- [5] C. Cheng and W. E. Bailey, Sub-micron mapping of GHz magnetic susceptibility using scanning transmission x-ray microscopy, *Appl. Phys. Lett.* **101**, 182407 (2012)
- [6] G. A. Prinz, Magnetoelectronics, *Science* **282**, 1660 (1998)
- [7] F. J. Albert, N. C. Emley, E. B. Myers, D. C. Ralph, and R. A. Buhrman, Quantitative study of magnetization reversal by spin-polarized current in magnetic multilayer nanopillars, *Phys. Rev. Lett.* **89**, 226802 (2002)
- [8] S. I. Kiselev, J. C. Sankey, I. N. Krivorotov, N. C. Emley, R. J. Schoelkopf, R. A. Buhrman, and D. C. Ralph, Microwave oscillations of a nanomagnet driven by a spin-polarized current, *Nature* **425**, 380 (2003)
- [9] V. E. Demidov, S. Urazhdin, H. Ulrichs, V. Tiberkevich, A. Slavin, D. Baither, G. Schmitz, and S. O. Demokritov, Magnetic nano-oscillator driven by pure spin current, *Nature Mat.* **11**, 1028 (2012)

- [10] J. Jorzick, S. O. Demokritov, B. Hillebrands, M. Bailleul, C. Fermon, K. Y. Guslienko, A. N. Slavin, D. V. Berkov and N. L. Gorn, Spin wave wells in nonellipsoidal micrometer size magnetic elements, *Phys. Rev. Lett.* **88**, 047204 (2002)
- [11] E. C. Stoner and E. P. Wohlfarth, A mechanism of magnetic hysteresis in heterogeneous alloys, *Phil. Trans. R. Soc. Lond. A* **240**, 599 (1948)
- [12] N. D. Rizzo, M. DeHerrera, J. Janesky, B. Engel, J. Slaughter, and S. Tehrani, Thermally activated magnetization reversal in submicron magnetic tunnel junctions for magnetoresistive random access memory, *Appl. Phys. Lett.* **80**, 2335 (2002)
- [13] T. Matcovich, H. S. Belson, and N. Goldberg, Resonant frequency shift in ellipsoidal samples, *J. Appl. Phys.* **32**, S163 (1961)
- [14] Y. Acremann, C. H. Back, M. Buess, O. Portmann, A. Vaterlaus, D. Pescia, and H. Melchior, Imaging precessional motion of the magnetization vector, *Science* **290**, 492 (2000)
- [15] I. Neudecker, M. Klaui, K. Perzlmaier, D. Backes, L. J. Heyderman, C. A. F. Vaz, J. A. C. Bland, U. Rudiger, and C. H. Back, Spatially resolved dynamic eigenmode spectrum of Co rings, *Phys. Rev. Lett.* **96**, 057207 (2006)
- [16] S. Mansfeld, J. Topp, K. Martens, J. N. Toedt, W. Hansen, D. Heitmann, and S. Mendach, Spin wave diffraction and perfect imaging of a grating, *Phys. Rev. Lett.* **108**, 047204 (2012)
- [17] V. E. Demidov, M. Buchmeier, K. Rott, P. Krzysteczko, J. Munchenberger, G. Reiss, and S. O. Demokritov, Nonlinear hybridization of the fundamental eigenmodes of microscopic ferromagnetic ellipses, *Phys. Rev. Lett.* **104**, 217203 (2010)

- [18] T. Bracher, P. Pirro, J. Westermann, T. Sebastian, B. Lagel, B. Van de Wiele, A. Vansteenkiste, and B. Hillebrands, Generation of propagating backward volume spin waves by phase-sensitive mode conversion in two-dimensional microstructures, *Appl. Phys. Lett.* **102**, 132411 (2013)
- [19] W.Chao, B.Harteneck, J.Liddle, E.Anderson, and D.Attwood, Soft X-ray microscopy at a spatial resolution better than 15 nm, *Nature* **435**, 1210 (2005)
- [20] S.-B. Choe, Y. Acremann, A. Scholl, A. Bauer, A. Doran, J. Stohr, and H. A. Padmore, Vortex coredriven magnetization dynamics, *Science* **304**, 420 (2004)
- [21] B. Van Waeyenberge, A. Puzic, H. Stoll, K. W. Chou, T. Tyliczszak, R. Hertel, M. Fahnle, H. Bruckl, K. Rott, G. Reiss, I. Neudecker, D. Weiss, C. H. Back, and G. Schutz, Magnetic vortex core reversal by excitation with short bursts of an alternating field, *Nature* **444**, 461 (2006)
- [22] J. Stohr, Y. Wu, B. D. Hermsmeier, M. G. Samant, G. R. Harp, S. Koranda, D. Dunham and B. P. Tonner, Element-specific magnetic microscopy with circularly polarized X-rays, *Science* **259**, 658 (1993)
- [23] D. A. Arena, Y. Ding, E. Vescovo, S. Zohar, Y. Guan, and W. E. Bailey, A compact apparatus for studies of element and phase-resolved ferromagnetic resonance, *Rev. Sci. Instrum.* **80**, 083903 (2009)
- [24] nmag.soton.ac.uk/nmag/
- [25] M. Bailleul, Shielding of the electromagnetic field of a coplanar waveguide by a metal film: implications for broadband ferromagnetic resonance measurements, *Appl. Phys. Lett.* **103**, 192405 (2013)

Author contributions

C.C. fabricated the samples, carried out micromagnetic simulations, analyzed data, and wrote the paper; both authors participated in design of the experiment and the samples, measurements of the TR-STXM and interpretation of the data.

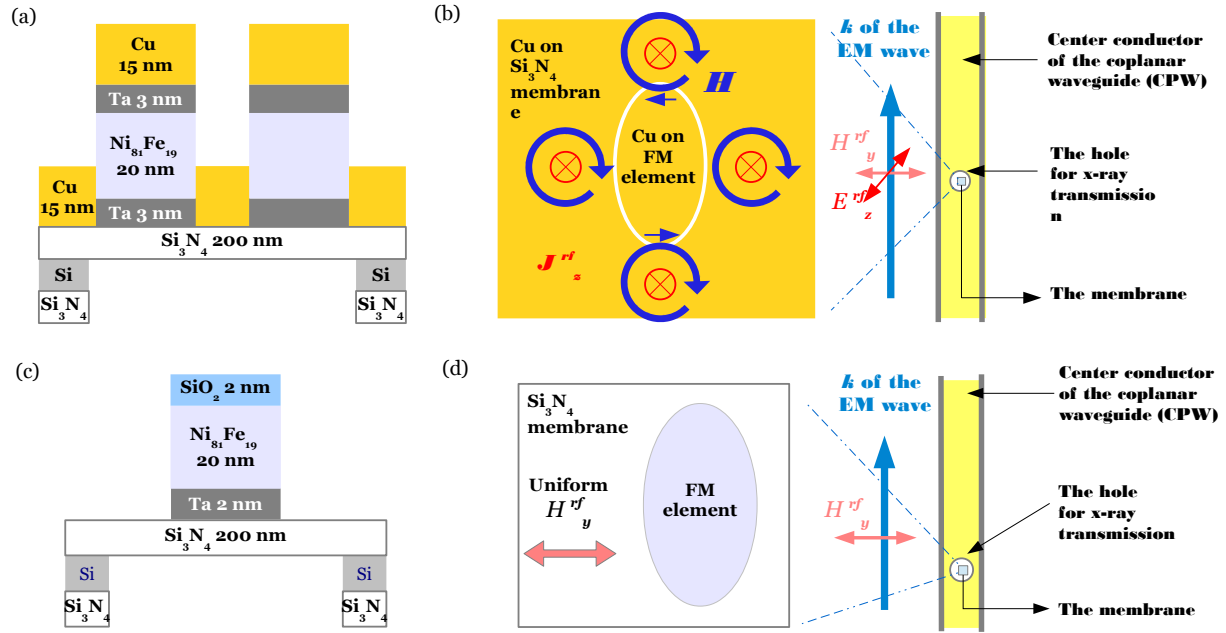
Figure legends

Fig.1 Sample structures. (a) Layer structure of the first sample type (*I*) for odd excitation; the 15 nm Cu layer covers the whole wafer. (b) The electrical field (E_z^{rf}) from the CPW, perpendicular to the sample plane, drives vertical rf current (J_z^{rf}) in the Cu layer, which induces antisymmetric rf magnetic field (H) at the tips of the ferromagnetic (FM) ellipse. (c) Layer structure of the second sample type (*II*) for even excitation. (d) The CPW imposes a uniform rf magnetic field over the sample.

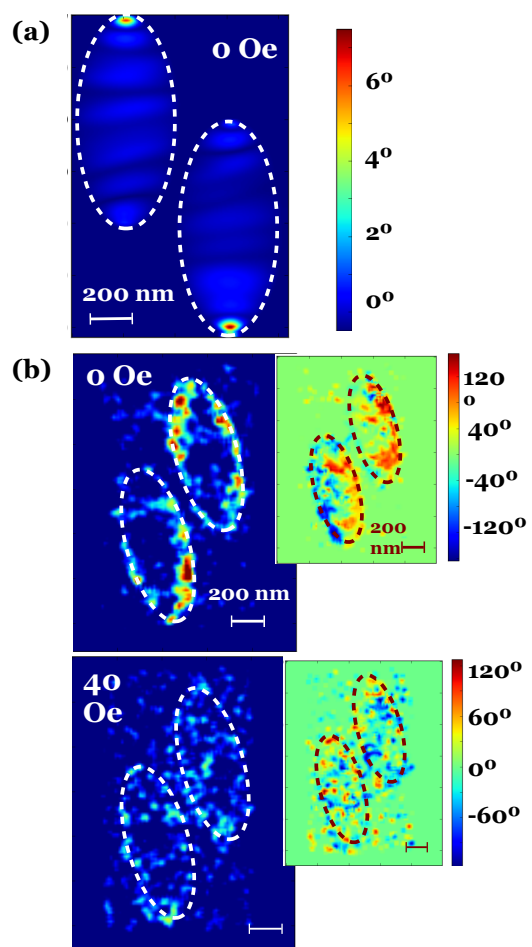
Fig.2 Magnetization amplitude and phase responses, $1000 \text{ nm} \times W=500 \text{ nm}$, $600 \text{ nm} \times 20 \text{ nm}$ ellipses, 2 GHz excitation. (a) The 'edge' mode under odd rf excitation in (*A,I*) at 2 GHz. Left image: simulated magnetization precession cone angle under zero bias (0 Oe); right: experimental data of the cone angle (upper panel) and the phase (lower panel), under different bias along the long axis. Pink line across the phase maps: guide for the eye to show the symmetry of the phase about the midline of the element. (b) The 'edge' mode under even rf excitation, zero bias (0 Oe) in (*A,II*); the phase map is symmetric about the midline. (c) A cross-over from the 'edge' mode to the 'uniform' mode in (*B,I*) at 2 GHz; demonstrating distinctive spin-wave mode pattern.

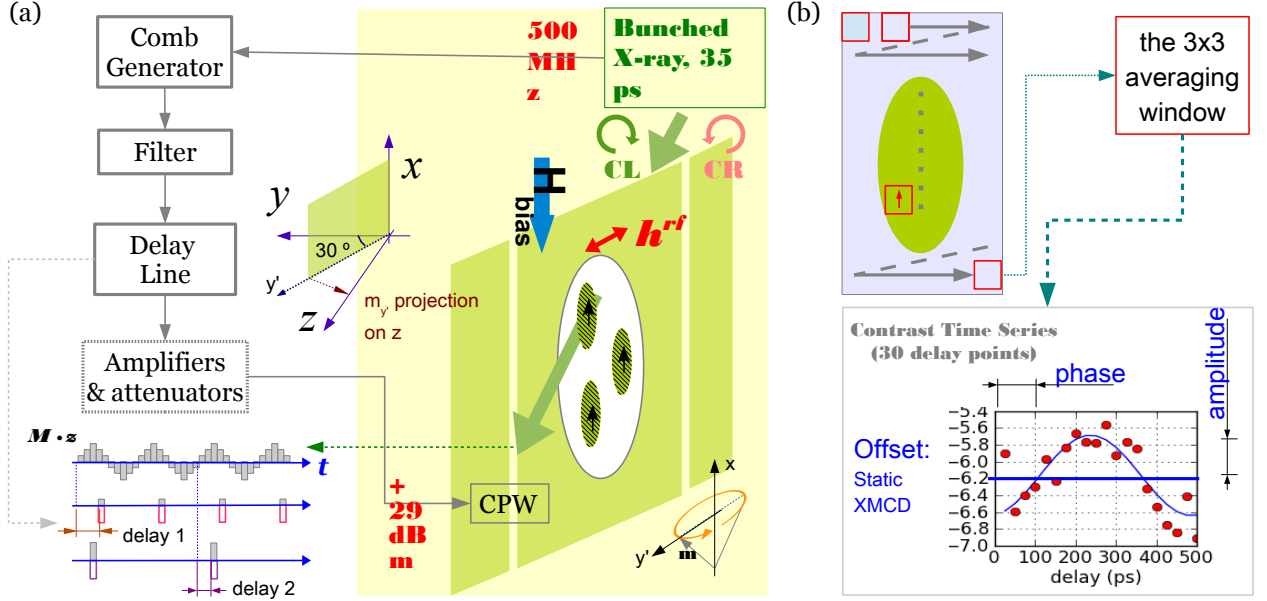
Fig.3 Dynamics (2 GHz) in a pair of ellipses. (a) Simulated magnetization precession amplitude in a pair of $1000 \text{ nm} \times 500 \text{ nm} \times 20 \text{ nm}$ $\text{Ni}_{81}\text{Fe}_{19}$ ellipses, at 2 GHz excitation and zero bias; the amplitude in the middle of the pair is reduced. (b) Experimental data at 2 GHz excitation for zero bias (0 Oe), showing reduced amplitude in the middle, and 40 Oe bias (off resonance).

Fig.4 Experiment methods. (a) Experimental setup, rf circuit for TR-STXM; (b) extracting amplitude and phase information at each sample point.



Figures





Supplementary information

Even and odd excitations First we give the simplest estimation of the direct rf magnetic field from the CPW, which is the case for even excitation. The custom designed CPW has a $400\text{ }\mu\text{m}$ wide center conductor and a characteristic impedance of $50\text{ }\Omega$. At $+29\text{ dBm}$ input power the current is $\sim 0.12\text{ A}$. For sample/CPW distance of $100\text{ }\mu\text{m}$, the estimated H^{rf} is 1.5 Oe .

In the case of odd excitation, the amplitude of the electrical field in the 15 nm Cu layer is $E_0 = (\omega/K)\mu H_0$, where $K = \omega\sqrt{\epsilon\mu\sqrt{1 + [\sigma/(\epsilon\omega)]^2}}$. For Cu at 2 GHz we approximate ω/K as $\sqrt{\omega/(\mu\sigma)}$ and have $E_0 = \mu H_0\sqrt{\omega/(\mu\sigma)} = H_0\sqrt{2}/(\sigma\delta)$, where $\delta = \sqrt{2/(\omega\mu\sigma)}$ is the skin depth. Using $H^{eddy} = \sigma E_0\pi a^2/(2\pi a)$, where a is the radius of a circular disk, we have $H^{eddy} = \frac{1}{\sqrt{2}}H_0(a/\delta)$. We take $a = 10\text{ }\mu\text{m}$ since the ellipses are separated by $10\text{ }\mu\text{m}$; the skin depth for $\sigma_{Cu} = 5.8 \times 10^7\text{ S/m}$ at 2 GHz is $1.48\text{ }\mu\text{m}$. Therefore we estimate that the transverse magnetic field induced by the electrical field in Cu, H^{eddy} , is about 5 times

the value of the direct H^{rf} from the CPW.